SYNTHESIS AND CHARACTERIZATION OF A NONIONIC SURFACTANT AS A CORROSION INHIBITOR FOR STEEL IN 1.0 M HCL.

S. SOLIMAN
Chemistry Department, Faculty of Science, Al -Azhar University, Cairo, Egypt.

M. METWALLY
Chemistry Department, Faculty of Science, Al -Azhar University, Cairo, Egypt.

S. SELIM
Chemistry Department, Faculty of Science, Al -Azhar University, Cairo, Egypt.

M. BEDAIR
*Chemistry Department, Faculty of Science, Al -Azhar University, Cairo, Egypt.*

SYNTHESIS AND CHARACTERIZATION OF A NONIONIC SURFACTANT AS A CORROSION INHIBITOR FOR STEEL IN 1.0 M HCL.

S.A. SOLIMAN, M.S. METWALLY, S.R. SELIM, AND M.A. BEDAIR[(*)]

Chemistry department, Faculty of science, Al-Azhar University.
(*)Corresponding author: m_bedier@yahoo.com, Mobile: +201014134321

Abstract

Synthesis, adsorption and corrosion inhibiting effect of new nonionic surfactant consisting of 3-[(4-Dimethylamino-benzylidene)-amino]-4-hydroxy-benzenesulphonic acid as hydrophobic part and poly ethylene glylcol (poly ethylene oxide) on steel in 1.0 M HCl was investigated using weight loss and potentiodynamic polarization techniques. The experimental findings revealed that this compound inhibited the corrosion reaction in 1.0 M HCl environment. The results indicated that this surfactant was adsorbed on the metal/solution interface. A theoretical study of the adsorption behavior of this compound was carried out in the framework of the semiempirical (SE) and molecular dynamics (MD).

1. Introduction

Acidization of petroleum oil well is one of the important stimulation techniques for enhancing oil production. It is brought about by using a kind of solution of hydrochloric acid. To reduce the aggressive attacks of acid on tubing and casing materials, inhibitors were incorporated to acid solution during acidizing process [1]. The efficiency of an organic compound as an inhibitor is mainly dependent on its ability to get adsorbed on metal surface which consists of a replacement of water molecules at a corroding interface as seen in the following equaton:

$$Org_{(Sol)} + nH_2O_{(ads)} \rightarrow Org_{(ads)} + nH_2O_{(Sol)}$$
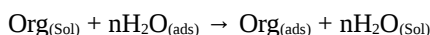
The adsorption of these compounds is influenced by the electronic structure of inhibiting molecules, steric factor, aromaticity and electron density at donor site, presence of functional groups such as –CHO, –N=N–, R-OH, etc., molecular area and molecular weight of the inhibitor molecule [2–5]. Experimental means are useful to explain the inhibition mechanism but they are often expensive and time-consuming. Ongoing hardware and software advances have opened the door for powerful use of theoretical chemistry in corrosion inhibition research. Several quantum chemical methods and molecular modeling techniques have been performed to correlate the inhibition efficiency of the inhibitors with their molecular properties [6-12]. The present work is aimed to study the inhibition efficiency of the synthesized Schiff base surfactant and calculate the quantum chemical parameters of

this compound. Furthermore, the interaction energy of the investigated inhibitor on the steel surface will be studied to discuss the inhibition mechanism.

2. Materials and Experimental Methods

2.1. Materials

Tests were performed on steel of the following composition: (0.11% C, 0.45% Mn, 0.04% P, 0.05% S, 0.25% Si, and the remained is Fe).

2.2. Inhibitor

This Schiff base surfactant was prepared through two steps; the first one is Schiff base reaction between 3-amino-4-hydroxy benzenesulfonic acid and 4-N, N dimethyl amino benzaldehyde in the molar ratio of 1:1, each reactant was dissolved in 50 ml ethyl alcohol and refluxed for 1 hour then the reaction mixture was left to cool and filtered. The product was washed and dried to give crystals of the produced Schiff base. The second step is esterfication of the Schiff base produced with poly ethylene glycol (M.wt =300) with 1:1 molar ratio using xylene as solvent and p-toluene sulphonic acid as a dehydrating agent refluxed for 6 hours. The product was washed and dried to give crystals of non ionic surfactant (Scheme 1).
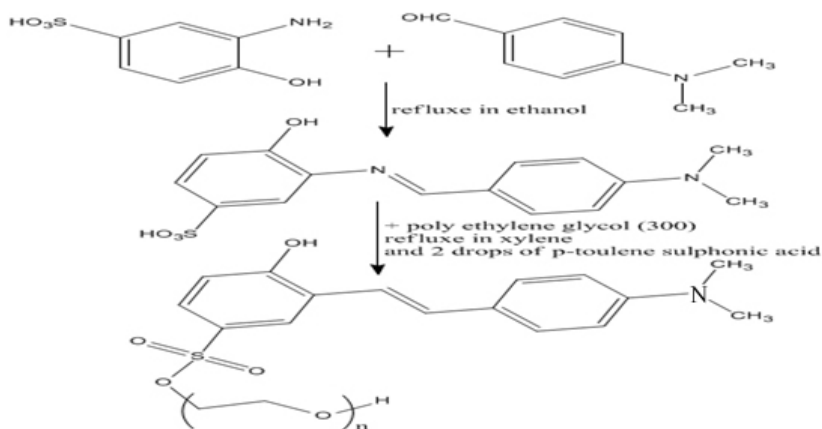
Scheme1. Synthetic route of the studied Schiff base non ionic surfactant.

2.3. Solutions

The aggressive solution, 1.0 M HCl, was prepared by dilution of analytical grade 37% HCl with distilled water. The concentrations of the prepared surfactant used were: 1×10^{-4}, 3×10^{-4}, 5×10^{-4}, 7×10^{-4}, and 9×10^{-4} M. All solutions were prepared using distilled water.

2.4. Electrochemical measurements

Conventional three-electrodes glass cell with a platinum counter-electrode and a saturated calomel electrode (SCE) as a reference was used. Steel rod as a working electrode was fitted into a polytetrafluoroethylene (PTFE) holder exposing only 1.0 cm^2 surface to the solution. The exposure surface was abraded with different grades of emery paper, degreased with acetone [13], washed with bidistilled water and finally dried. The experiments were carried out at constant temperature (within ±1 ^{o}C).

2.5. Weight loss measurements

The steel sheets of 6.0 cm ×2.5 cm × 0.3 cm with an exposed total area of 35.1 cm^2 were used for weight loss measurements. They were abraded with different grades of emery paper washed with distilled water, and dried in acetone and warm air. The precleaned and weighed coupons were suspended in beakers containing the test solutions using glass hooks and rods. Tests were conducted under total immersion conditions in 100 ml of the aerated test solutions. To determine weight loss with respect to time, test coupons were retrieved at 24 h intervals progressively for 96 h, scrubbed with a bristle brush, washed, dried and reweighed. The weight loss was taken as the difference between the initial and final weights of the coupons.

2.6. Quantum chemical calculations:

Complete geometrical optimizations of the investigated molecules were performed initially using semi-empirical PM6 method. Total structure optimization is implemented by means of Gaussian 09 program package [14]. Frontier molecular orbitals (HOMO and LUMO) could be used to predict the adsorption centers of the inhibitor molecule. For the simplest transfer of electrons, adsorption should occur at the part of the molecule where the softness, σ, which is a local property, has the highest value. According to Koopman's theorem [15], the E_{HOMO} and E_{LUMO} of the inhibitor molecule are related to the ionization potential, I, and the electron affinity, A, by the following relations:

$$I = -E_{HOMO} \qquad\qquad A = -E_{LUMO}$$

Absolute electronegativity, X, and absolute hardness, η, of the inhibitor molecule are given by [16]:

$$X = (I+A)/2 \qquad\qquad \eta = (I-A)/2$$

2.7.   Molecular dynamic simulation:

Molecular simulation studies (MD) were performed using Materials studio 4.3 software from Accelrys Inc. [17] which has been used to build surfactant molecule and Fe (1 1 1) surface (as steel) using the sketching tools in Materials Visualizer. COMPASS (Condensed Phase Optimized Molecular Potentials for Atomistic Simulation Studies) [18] is the first ab initio force field that enables accurate and simultaneous prediction of chemical properties (structural, conformational, vibrational, etc.) and condensed-phase properties (equation of state, cohesive energies, etc.) for a broad range of chemical systems. The first step in this computational study is the preparation of a model of molecules which will adsorb on the surface with optimized geometry (i.e. energy minimized). The MD simulation of the interaction between the surfactant molecule and the Fe surface (1 1 1) was carried out in a simulation box (22.90 ×57.26 ×26.68 Å) with periodic boundary conditions to model a representative part of an interface devoid of any arbitrary boundary effects. The box consists of a Fe slab and a vacuum layer of 15.00 Å heights. The interaction energy $E_{Fe-inhibitor}$ of the steel surface with the inhibitor was calculated according to the following equation:

$$E_{Fe-inhibitor} = E_{complex} - (E_{Fe} + E_{inhibitor})$$

Where $E_{complex}$ being the total energy of Fe crystal together with the adsorbed inhibitor molecule. E_{Fe} and $E_{inhibitor}$ being the total energy of Fe crystal and free inhibitor molecules, respectively. The binding energy was the negative sign value of interaction energy, $E_{binding} = - E_{Fe-inhibitor}$.

3. Results and Discussion:

3.1.   Confirmation of the chemical structure of the synthesized inhibitor:

The chemical structure of the prepared surfactant was confirmed by IR, ^{1}HNMR, Mass and (C, H, N, S) analysis and the results are shown in Figs. 1, 2 and 3, respectively and Tables 1, 2.

3.1.1. IR Spectrum
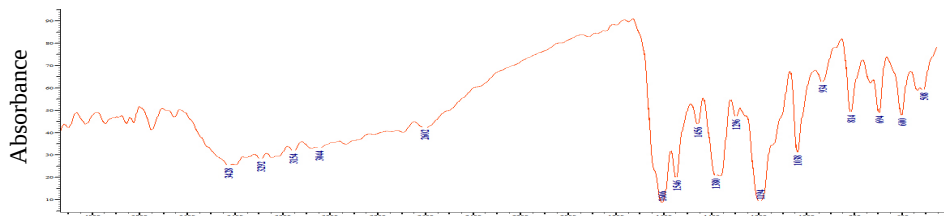
Fig.1. IR of the synthesized Schiff base surfactant

IR spectrum of the synthesized compound showed the following absorption bands located at 694 cm^{-1} (CH$_2$ rocking), 1038 cm^{-1} (S-O,S=O) stretching, 1194 cm^{-1} (C-N) alkyl stretching, 1296 cm^{-1} (C-N) aryl stretching, 1380cm^{-1} (CH$_2$ deformation), 1456 cm^{-1} (CH$_2$ bending), 1546 cm^{-1} (C=C) aromatic ring stretching, 1606 cm^{-1} (C=N) and 3428 cm^{-1} (phenolic OH). The FTIR spectra confirmed the expected function groups in the synthesized Schiff base surfactant. These bands are listed in **Table 1.**

Table 1. IR bands of the synthesized inhibitor.

Assignment	Wave number (cm^{-1})	Assgnment	Wave number (cm^{-1})
(CH$_2$)$_n$– rocking.	694	Symmetric bending (CH$_2$)	1456
(S-O,S=O) stretching	1038	(C=C) aromatic ring stretching	1546
(C-N) alkyl stretching	1194	(C=N)	1606
(C-N) aryl stretching	1296	Phenolic OH group	3436
(CH$_2$) deformation	1380		

3.1.2. ^{1}HNMR Spectrum

^{1}HNMR (DMSO) spectrum of the synthesized inhibitor is represented in Fig. 2.
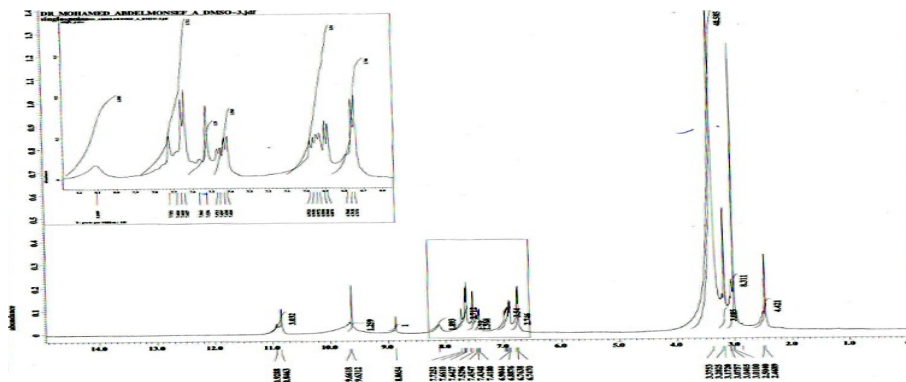
Fig. 2. ^{1}HNMR spectrum of inhibitor.

^{1}HNMR spectrum showed different bands at: δ=10.8463ppm (s, 1H, (phenolic)–O**H**; δ=9.6312 ppm (s, 1H, N=C**H**); δ=7.7573-7.8689 ppm (d, 2H, m-phenolic nucleus); δ=7.7084–7.7573 ppm (d, 2H, o-benzelidine nucleus); δ=7.4501–7.5571 ppm (t, 3H, m,p-benzelidine nucleus; δ=3.3753-3.4746 ppm (t, 20H, OSO(OCH$_2$CH$_2$)n); and δ=2.3711-2.4704ppm (t, 2H, OCH$_2$CH$_2$OH). The data of

^{1}HNMR spectrum confirmed the expected hydrogen proton distribution in the synthesized inhibitor.

3.1.3. Mass Spectrum

The mass spectrum of the synthesized inhibitor, Fig. 3, illustrated a molecular ion peak at m/z 610 (24.39%) together with other significant peaks, which are observed at m/z (intensity %): base peak at 148 (100 % $HN=CH-ph-N(CH_3)_2$),77 (24.15 % C_6H_5), 133 (29.02 % $CH-ph-N(CH_3)_2$), 173 (23.90 % ($CH_2=CH-N=CH-ph-N(CH_3)_2$), 242 (18.54 % $HO-ph-N=CH-ph-N(CH_3)_2$), 272 (29.76 % ((p,HS),(o,HO)-$ph-N=CH-ph-N(CH_3)_2$)) and 303 (18.54 % ((p,O_2S),(o,HO)-$ph-N=CH-ph-N(CH_3)_2$)). Data of mass spectrum confirmed the chemical structure of the synthesized Schiff base surfactant.
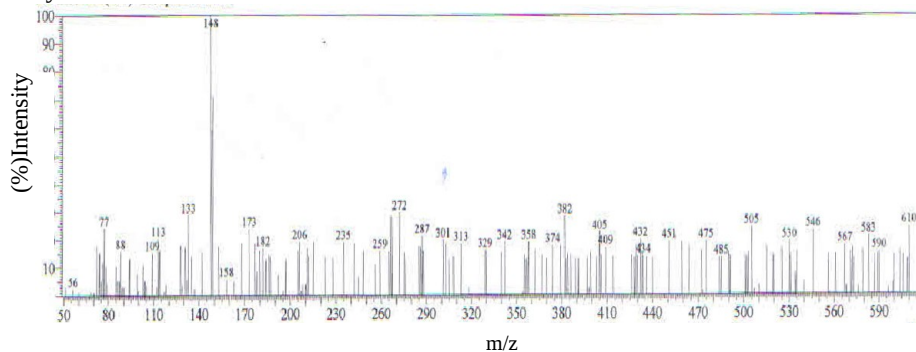
Fig.3. Mass spectrum of the synthesized Schiff base surfactant

3.1.4. C, H, N and S Elemental Analysis

The results C, H, N and S elemental analysis indicated the following data

Table.2. C, H, N and S elemental analysis of the synthesized Schiff base surfactant

Element %	C,%	H,%	N,%	S,%
Found	53.98	5.24	5.34	6.43
Calculated	54.71	6.89	4.56	5.22

3.2.   Electro Chemical Measurements
3.2.1. Open Circuit Potential:

The variation of the OCP of steel was followed as a function of time in aerated non-stirred 1.0 M HCl solution in the absence and presence of various concentrations of the selected surfactant. The results obtained are depicted in Fig. 4.
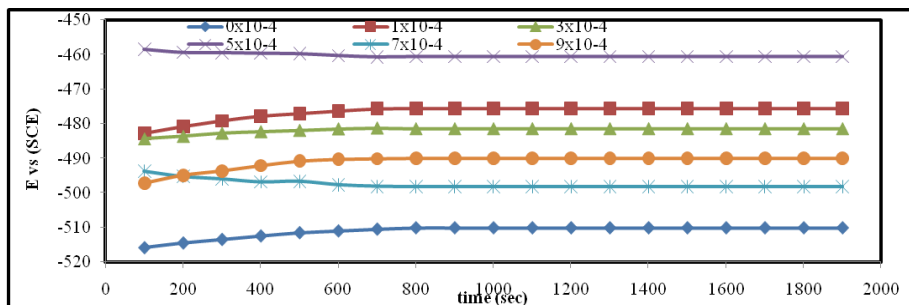
Fig. 4. Variation of the OCP of steel with time of immersion in 1.0 M HCl solutions in the absence and presence of various znnnnnconcentrations of the surfactant.

In inhibitor-free HCl solution (blank), the OCP changed quickly towards more negative values, indicating that the initial dissolution process of the pre-immersion, air formed oxide film and the attack on the bare metal [19].

A steady potential was readily attained, corresponding to the free corrosion potential, E_{corr}, of the metal [20]. Addition of surfactant drifts the steady state E_{corr} to less negative values without changing the general shape of the OCP vs time plots. According to Riggs [21], the classification of a compound as an anodic or cathodic type inhibitor is feasible when the OCP displacement is at least 85 mV in relation to that one measured for the blank solution. However from Fig. 4, the positive shift in E_{corr} is less than 55 mV with increasing inhibitor concentration. This positive shift in E_{corr} is too small for a reasonable classification based on OCP results. So polarization experiments has been done to show that the tested surfactant affects anodic and (or) cathodic parts of the polarization curves.

3.2.2. Polarization Measurements:

Polarization data had been treated by Tafel and Evans methods

a- Tafel Method

An anodic and cathodic polarization curves of steel in 1.0 M HCl solutions in the absence and presence of various concentrations of the inhibitor is shown in Fig.5. In the presence of inhibitor at high concentrations (7×10^{-4} and 9×10^{-4} M), the E_{corr} values are slightly shifted toward the more negative direction in comparison to that obtained in the absence of inhibitor. Both of the anodic and cathodic current densities are decreased by addition of inhibitor, but the cathodic curves are affected

to a greater extent. This result suggests that the inhibitor suppressed both the anodic and cathodic reactions, although mainly the cathodic one [22]. While at lower concentrations (1×10^{-4}, 3×10^{-4}, and 5×10^{-4} M), the E_{corr} values are slightly shifted toward the positive values in comparison to those obtained in the absence of the inhibitor and the anodic inhibiting effect becomes more pronounced. These findings suggest that the inhibiting action of the inhibitor and the adsorption mode on metal surface are highly affected by the concentration of the inhibitor. It may be due to that the inhibitor at low concentrations (surfactant) is completely adsorbed on metal surface by both hydrophobic and hydrophilic parts while at high concentrations only hydrophobic part adsorb on surface.
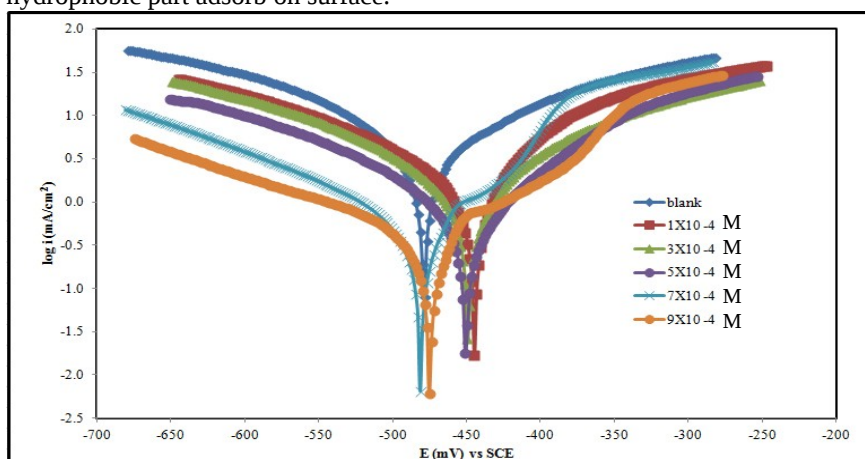
Fig.5. Tafel polarization curves of steel in 1.0 M HCl solutions containing various concentrations of nnmminhibitor.

The electrochemical parameters such as corrosion potential (E_{corr}), corrosion current density (i_{corr}), cathodic Tafel slope (βc) and anodic Tafel slope (βa) obtained from the polarization curves and the corresponding inhibition efficiency (η_p) values at different inhibitor concentrations are reported in **Table 3.**

Table 3. Electrochemical parameters for steel in 1.0 M HCl solution containing different concentrations of the inhibitor.

Conc.	E_{corr} vs.SCE(mV)	I_{corr} (mA cm^{-2})	β_a (mV dec^{-1})	β_c (mV dec^{-1})	Rp (Ω.cm^2)	C.R(m m y^{-1})	Θ	η_p%
0×10^{-4}	-478.4	8.2353	250.6	-218.3	5.73	96.32	-----	----
1×10^{-4}	-444.8	4.0749	158.3	-246.5	12.58	47.66	0.505	50.52
3×10^{-4}	-448.7	2.3082	167.0	-180.6	17.15	26.99	0.719	71.97
5×10^{-4}	-450.0	1.4966	130.2	-181.6	29.13	17.50	0.818	81.82
7×10^{-4}	-480.7	0.6156	70.8	-150.0	36.38	7.200	0.925	92.52
9×10^{-4}	-474.5	0.4102	88.7	-184.9	49.47	4.798	0.950	95.02

Inspection of the η_p values revealed that inhibition efficiency increases with increasing concentration of inhibitor (Table 3 and Fig.5.). It can be observed that the values of corrosion current density (i_{corr}) of steel in the presence of inhibitor are lower than that for the inhibitor-free solution. This suggests that the inhibitor was adsorbed on the metal surface by blocking more of the active sites of the metal surface. The increase in inhibition efficiencies observed at higher inhibitor concentrations indicates that more inhibitor molecules were adsorbed on the metal surface, thus providing wider surface coverage and that this compound acted as an adsorption inhibitor.

b- Evans method

The polarization data was also treated using Evans method. Evans parameters are listed in Table 4 and Fig. 6.represents the application of Evans diagram principle for the influence of different concentrations of inhibitor on the cathodic and anodic polarization curves for steel in 1.0 M HCl. The solid and dotted curves represent the blank (no inhibitor) and inhibited polarization curves, respectively. It is clear from the constructed Evans diagrams that the inhibitor function is mixed type inhibitor (both cathodic and anodic) but highly cathodic more than anodic since the presence of this inhibitor increases the cathodic overpotential and shifts the corrosion potential E_{corr} to more negative values indicating that the inhibitor retards the hydrogen evolution reaction at concentrations 1×10^{-4}, 7×10^{-4} and 9×10^{-4} M. However, at concentrations 3×10^{-4} and 5×10^{-4} M the inhibitor behave mainly as mixed type, since the addition of the inhibitor to the acid solution increases both the anodic and cathodic overpotentials indicating that the presence of inhibitor retarded both anodic dissolution of the metal and cathodic evolution of hydrogen .

Table 4. Relative parameters derived from Evans diagrams for steel in 1.0 M HCl.

	Corrosion		cathod		anode		Efficiency
Conc.	$\Delta\varphi_{corr}$ (mV)	I_{corr} (mA cm^{-2})	$\Delta\varphi_c$(mV)	I_c (mA cm^{-2})	$\Delta\varphi_a$(mV)	I_a (mA cm^{-2})	η_p%
0×10^{-4}	-478.27	14.58	-----	----	-----	----	----
1×10^{-4}	-502.81	8.15	-476.01	13.97	-505.74	8.51	44.10
3×10^{-4}	-486.75	5.94	-457.81	9.51	-507.03	8.28	59.26
5×10^{-4}	-490.52	4.05	-457.01	9.33	-519.33	6.34	72.22
7×10^{-4}	-498.02	2.57	-470.19	12.48	-533.40	4.41	82.37
9×10^{-4}	-499.44	1.36	-447.11	7.14	-545.86	2.44	90.67
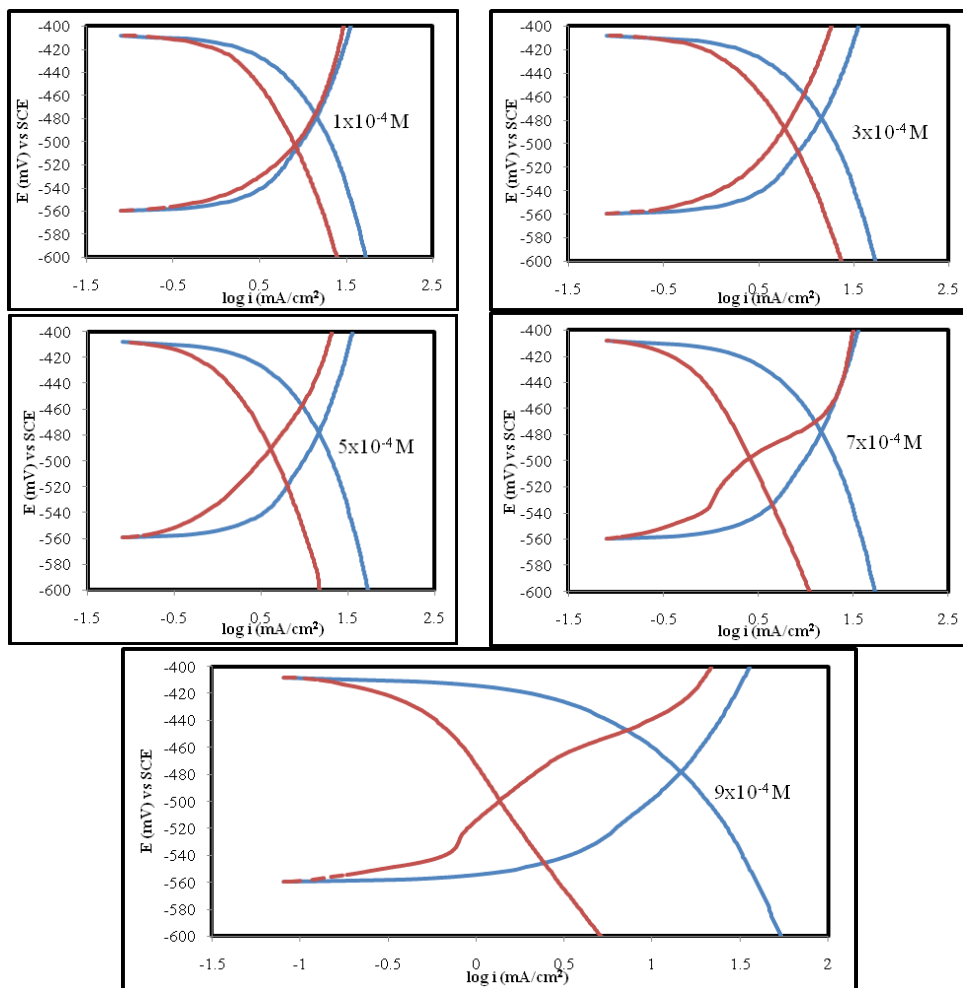
Fig. 6. Evans diagrams for steel in presence of different concentrations of the inhibitor.

3.3.   Weight Loss Measurements:

3.3.1. Influence of inhibitor concentrations on the corrosion rate:

The corrosion parameters such as corrosion rate (k), inhibition efficiency (η_w %) and surface coverage (θ) at different concentrations of the synthesized surfactant in 1.0 M HCl at different temperatures (30, 40 and 50 $^{\circ}$C) are listed in Table 5, which shows that the synthesized surfactant inhibits the corrosion of carbon steel at all concentrations in 1.0 M HCl, and the inhibition efficiency increases with increasing concentration of the synthesized surfactant. The results indicate also that the corrosion rate increased with exposure time and that surfactant actually retarded

steel corrosion at all concentrations in 1.0 M HCl which is shown in Fig. 7.(a, b and c).The relation between η_w % of steel and logarithm of the concentrations of the inhibitor is shown in Fig. 7.(d).

The value of corrosion rate was calculated from the following equation [23]:

$$k = \frac{\Delta W}{A.t}$$

Where k is the corrosion rate (mg.cm^{-2}.h^{-1}), ΔW is the loss of weight after corrosion (mg), A is the total area of the coupon (cm^2), and t is the corrosion time (h).

The degree of surface coverage (θ) and the inhibition efficiency, (η_w%), were calculated using the following equations [24, 25]:

$$\theta = \frac{k_o - k}{k_o}$$

$$\eta_w \% = \frac{k_o - k}{k_o} \times 100$$

Where k_o and k are the values of the corrosion rate without and with addition of the inhibitor, respectively.

Table 5. Weight loss data for steel in 1.0 M HCl without and with different concentrations of the synthesized surfactant at various temperatures (30, 40 and 50 ºC) .

Conc.(M) x10^{-4}	30 ºC			40 ºC			50 ºC		
	K(mg.cm^{-2}.h^{-1}) x 10^{-2}	θ	η_w(%)	K(mg.cm^{-2}.h^{-1}) x 10^{-2}	θ	η_w(%)	K(mg.cm^{-2}.h^{-1}) x 10^{-2}	θ	η_w(%)
0	15.86	--	--	66.29	--	--	76.25	--	--
1	7.98	0.49	49.66	30.41	0.54	54.11	31.74	0.58	58.37
3	4.19	0.73	73.54	11.44	0.83	82.73	7.61	0.90	90.03
5	2.79	0.82	82.35	3.87	0.94	94.15	3.46	0.95	95.45
7	1.56	0.90	90.10	2.67	0.959	95.96	2.43	0.968	96.80
9	1.12	0.93	92.93	2.47	0.962	96.27	2.20	0.971	97.11
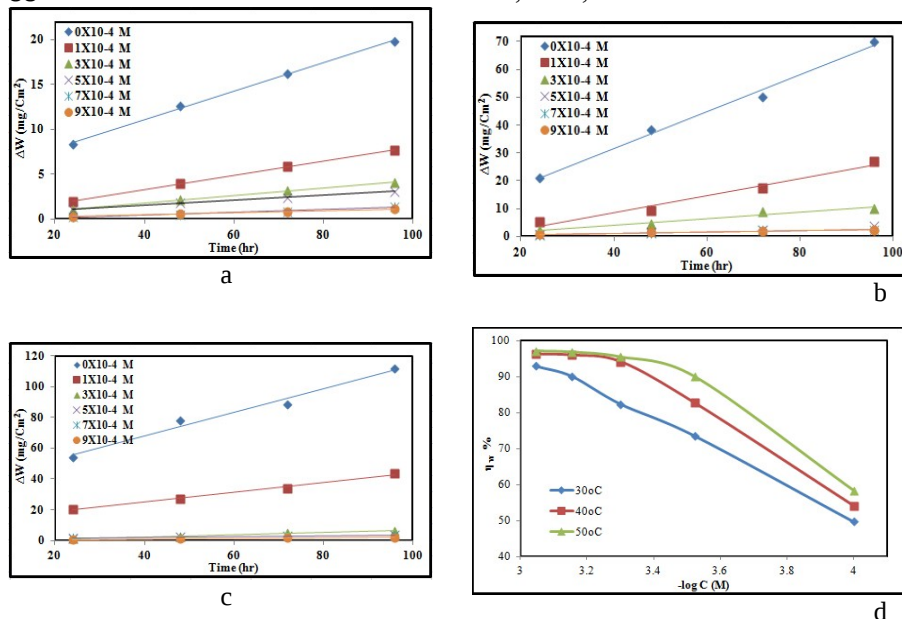
Fig.7. Variation of weight loss with exposure time for steel corrosion in 1.0 M HCl in the Presence and absence of nnnnnnnsurfactant at a (30), b (40) and c (50) °C (a, b and c); d is variation of inhibition efficiency with concentration.

3.3.2. Adsorption Consideration.

The adsorption of organic molecules provides information about the interaction among the adsorbed molecules themselves as well as their interaction with the electrode surface. The surface coverage (θ) was tested graphically for fitting a suitable adsorption isotherm as indicated in Fig. 8. Plotting C_{inh}/θ vs. C_{inh} yielded a straight line with a correlation coefficient (R^2) higher than 0.99 and a slope closed to 1. This indicates that the adsorption of this inhibitor can be fitted to a Langmuir adsorption isotherm which expressed as

$$\frac{C}{\theta} = \frac{1}{K_{ads}} + C$$

The strong correlation of the Langmuir adsorption isotherm may confirm the validity of this approach. The equilibrium constant (K_{ads}) for the adsorption–desorption process of this compound can be calculated from reciprocal of the intercept. The K_{ads} values are listed in Table 6. It is clear that, the large K_{ads} values indicate a strong adsorption of the synthesized inhibitor on the surface of steel and it increases as the temperatures an increase, which indicates that the inhibitor is

strongly adsorbed onto the steel surface at relatively higher temperatures. This may be due to the formation of coordinated bonds between the prepared surfactant and the d-orbital of iron on the surface of steel.
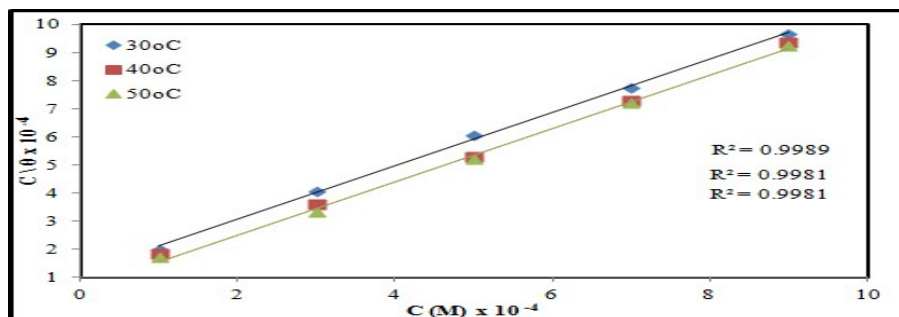
Fig.8. Langmuir adsorption plots for carbon steel in 1.0 M HCl at the presence of different concentrations of the inhibitor at different temperatures.

The adsorption heat was calculated according to the Van't Hoff equation [26]:

$$\ln K_{ads} = \left(-\frac{\Delta H_{ads}}{RT}\right) + \ const$$

Where ΔH_{ads} and K_{ads} are the adsorption heat and adsorptive equilibrium constant, respectively. It should be noted that - ΔH_{ads} / R is the slope of the straight line for plotting $\ln K_{ads}$ against 1/T Fig. 9. The positive values of ΔH_{ads} shows that, the adsorption of the inhibitors is an endothermic process [27], which indicates that, the inhibition efficiency increases with the increasing temperature. Such behavior can be interpreted on the basis that the increase in temperature resulted in an increase in the chemisorption of inhibitor molecules on the metal surface. The adsorption entropy ΔS_{ads} was obtained using the basic thermodynamic equation:

$$\Delta G_{ads} = \Delta H_{ads} - T \Delta S_{ads}$$

Values of K_{ads}, ΔH_{ads}, ΔG_{ads} and ΔS_{ads} are listed in Table (6) .Positive sign of ΔS_{ads}, as was obtained, since the endothermic adsorption process is always accompanied by an increase of entropy. This increase of entropy was the driving force of the adsorption of inhibitor on to carbon steel surface [28, 29].

Table 6. Thermodynamic parameters using Langmuir adsorption isotherm on steel surface in 1.0 M HCl containing different concentrations of the surfactant at different temperatures.

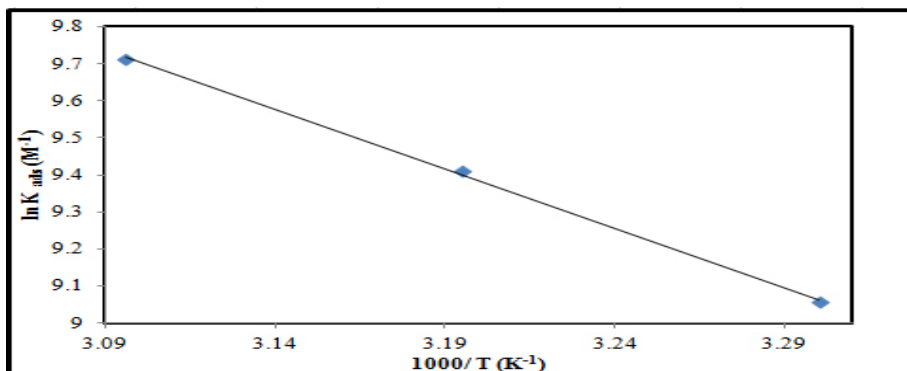| Temp °k	K_{ads} (KJ/mol)	ΔG_{ads} (KJ/mol)	ΔS_{ads} (J/mol .°k)	ΔH_{ads} (KJ/mol)
303	8.577	-32.93	196.9	26.73
313	12.221	-33.82	193.4	26.73
323	16.542	-34.58	189.8	26.73

Fig.9. plot of ln K $_{ads}$ against 1/T.

3.3.3. Effect of Temperatures:

In acid medium, the corrosion rate is related to temperature by Arrhenius equation:

$$\log k = \log A - \frac{E_a}{2.303\ RT}$$

Where k is the corrosion rate determined from weight loss measurements, E_a is the apparent activation energy and A is the Arrhenius constant. The apparent activation energy was determined from the slopes of log k against 1/T (Fig. 10) .
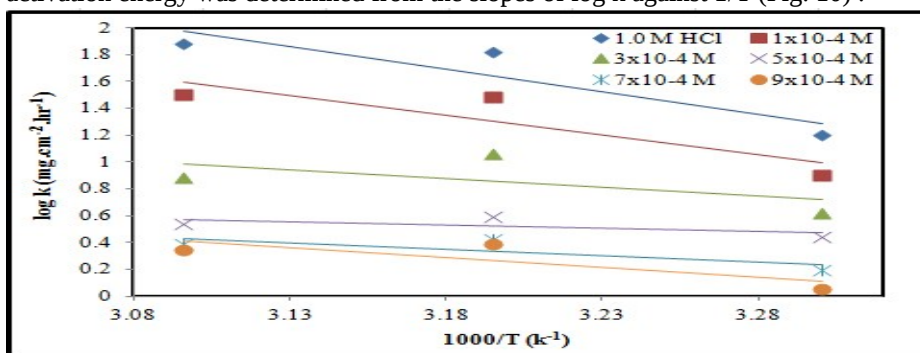

Fig. 10. Arrhenius plots of log k versus 1/T for carbon steel in 1.0 M HCl solution without and with different nnnnnn concentrations of the inhibitor.
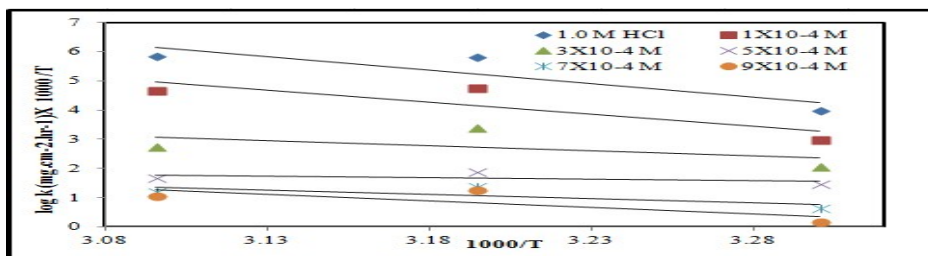
The values of enthalpy of activation ΔH^* and entropy of activation ΔS^* were obtained from the transition state equation

$$k = \left(\frac{RT}{Nh}\right) \exp\left(\frac{\Delta S^*}{R}\right) \exp\left(\frac{-\Delta H^*}{RT}\right)$$

Where h is the Planck's constant, N is the Avogadro's number, T is the absolute temperature and R is the universal gas constant. A plot of log (k/T) as a function of 1/T (Erying equation) Fig. 11.showed a straight line. ΔH^* and ΔS^* were calculated from the slope and intercept, respectively. The calculated values of the thermodynamic parameters of activation for the dissolution of steel at different temperatures are presented in Table 7. These data show that the values of both ΔH^* and ΔS^* in the presence of inhibitor increase over that of blank which means that the energy barrier of corrosion reaction in the presence of the inhibitor increases. The positive values of ΔH^* showed that the dissolution process is endothermic. The increase of value of ΔS^* (less negative) meaning that decrease in disorder is due to the molecules oriented on the surface and ordered by adsorption through the active centre.

Table 7. Activation parameters values for steel in 1.0 M HCl in the absence and presence of different concentrations of the inhibitor.

| Conc. (M) X 10 $^{-4}$	Ea (kJ mol^{-1})	ΔH^* (kJ mol^{-1})	ΔS^* (J mol^{-1} K^{-1})
0	64.43	76.69	202.65
1	56.72	68.80	168.44
3	24.88	28.32	27.37
5	8.94	8.33	45.24
7	18.30	23.02	3.34
9	27.85	37.06	39.58

Fig.11. Erying plots of the corrosion rate for steel in 1.0 M HCl in absence and presence of inhibitor at 30, 40 and nnnn 50 ∘C.

3.4. Scanning Electron Microscopy (SEM):

Immersion corrosion analysis of steel samples in the acidic solutions with and without the inhibitor was performed using SEM. SEM Jeol JSM-5400 was used for the experiments. SEM image of the steel specimens after immersion in 1.0 M HCl for 24 h is shown in Fig. 12a; the micrograph revealed that the surface was strongly damaged in absence of inhibitor. Fig. 12b shows the SEM image of another steel specimen after immersion for the same time interval in 1.0 M HCl containing 9 x 10^{-4} M of the prepared surfactant; the SEM images indicated that a protective film on the steel surface was responsible for the highest inhibition of corrosion in presence of the prepared surfactant.

a   b
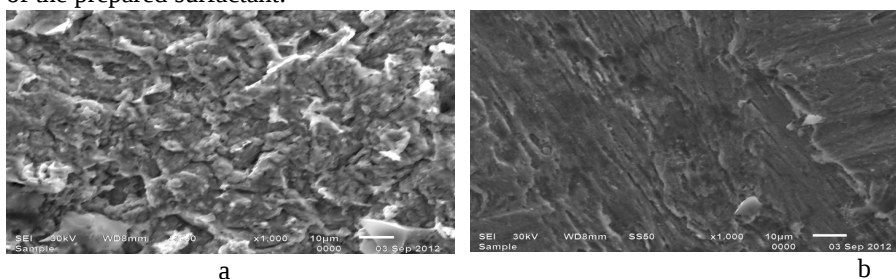
Fig. 12. SEM image of carbon steel surface after immersion for 24 h in 1.0 M HCl at 25 ºC in (a) absence and (b) presence of 9x10^{-4}M of inhibitor.

Energy dispersive x-ray (EDX) survey spectra were used to determine which elements were present on the steel surface before and after exposure to the inhibitor solution. The results are displayed in Fig. 13. For the electrode without inhibitor treatment (Fig. 13a), only iron was detected. However, in inhibited solution (Fig. 13b), the EDX spectra showed an additional line characteristic for the existence of C, O and S signals (due to the carbon, oxygen and sulpher atoms of the inhibitor). These data show that a carbonaceous material containing oxygen atoms and sulpher has covered the steel surface. This layer is undoubtedly due to the inhibitor, because the carbon signal and the high contribution of the oxygen signal are not present on the electrode surface exposed to uninhibited (see Fig. 13a).It is possible that the inhibitor surface film acted as a barrier to the diffusion of H^{+} ions from solution to electrode surface, which may increase the overpotential of the cathodic hydrogen evolution reaction. This surface film also increased the polarization resistance of anodic dissolution of steel. These results support the results obtained from chemical and electrochemical measurements.
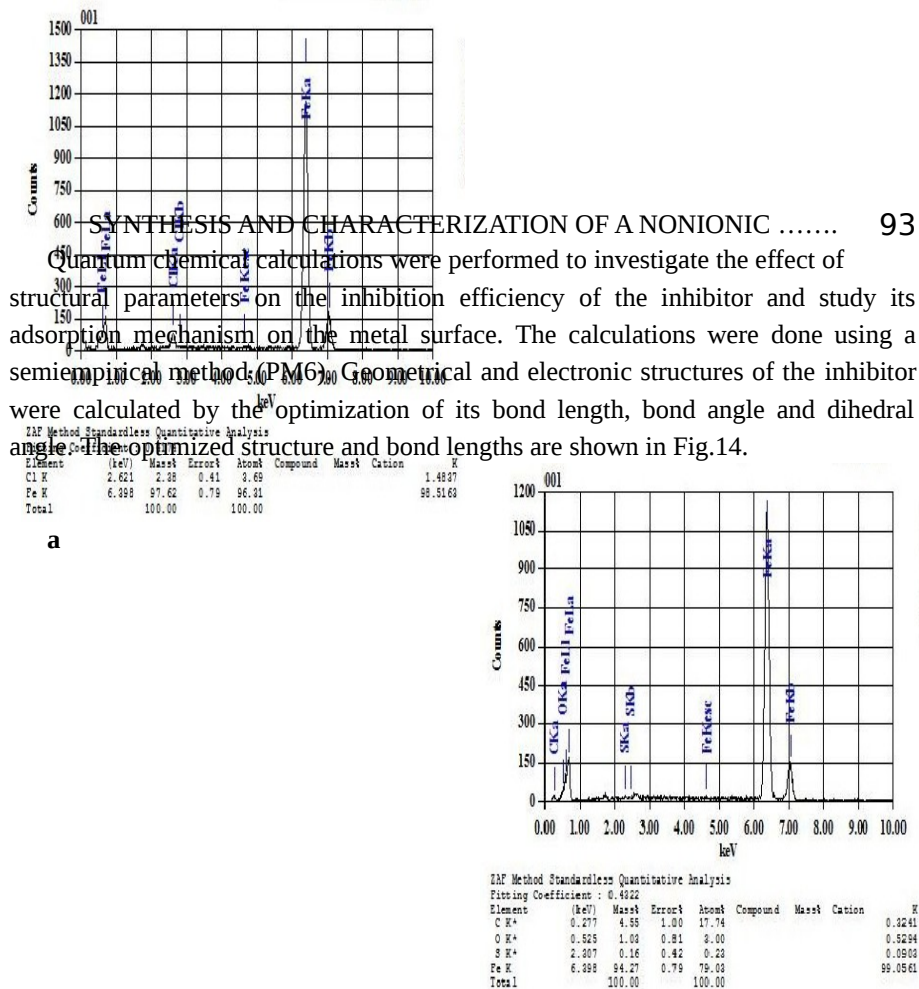
3.5.   Quantum Chemical Calculations:

Quantum chemical calculations were performed to investigate the effect of structural parameters on the inhibition efficiency of the inhibitor and study its adsorption mechanism on the metal surface. The calculations were done using a semiempirical method (PM6). Geometrical and electronic structures of the inhibitor were calculated by the optimization of its bond length, bond angle and dihedral angle. The optimized structure and bond lengths are shown in Fig.14.

a

b

Fig. 13. EDX spectra recorded for steel specimens immersed in 1.0 M HCl for 24 h in the absence (a) and (b) presence of 9x10^{-4} M of the inhibitor at 25 ºC.
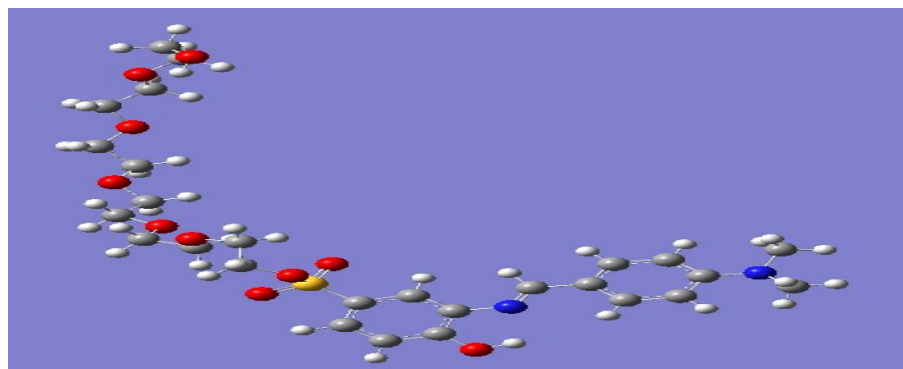

**Fig.14 .The optimized molecular structure and bond length
for the investigated compound.**

Table .7 presents the calculated quantum parameters for the inhibitor molecule. Frontier orbital theory is useful in predicting adsorption centers of the inhibitor

molecules responsible for the interaction with surface metal atoms [30, 31]. Terms involving the Frontier MO could provide dominative contribution, because of the inverse dependence of stabilization energy on orbital energy difference [30]. It has been reported in the literature that the higher the HOMO energy of the inhibitor, the greater the trend of offering electrons to vacant d orbital of the metal, and the higher the corrosion inhibition efficiency. In addition, the lower the LUMO energy, the easier the acceptance of electrons from metal surface; this means better inhibition efficiency [32]. The Frontier molecule orbital density distributions for inhibitor are shown in Fig. 15. Quantum chemical parameters revealed that the inhibitor has high HOMO and low LUMO (**Fig. 15)**. On the other hand, HOMO was mainly distributed on the area containing sulfur and nitrogen atoms. Thus, the area containing both sulfur and nitrogen atoms considered to be the primary site of the bonding [31]. So we can deduce that the inhibitor can interact with steel surface using a number of active centers forming a good protective layer on the steel surface, thus retarding further corrosion of the metal in hydrochloric acid solution.

Table 7.The calculated quantum chemical parameters of the inhibitor

Total energy (eV)	E_{HOMO} (eV)	E_{LUMO}(eV)	ΔE (eV)	μ(Deby)
-15.374	-7.733	-5.42	2.32	7.37

Fig. 15. The frontier molecule orbital density distributions of the inhibitor.

3.6.   Molecular Dynamic Simulations

Molecular dynamics were performed on a system comprising an inhibitor molecule and steel surface. The inhibitor molecule was optimized first and then run quench molecular dynamics using Monte Carlo simulations. Monte Carlo simulations help in finding the most stable adsorption sites on metal surfaces through finding the low energy adsorption sites on both periodic and non-periodic substrates or to investigate the preferential adsorption of mixtures of adsorbate components. Several outputs and descriptors calculated by the Monte Carlo simulation are presented in Table 8. The parameters presented in Table 8 include total energy, in kJ mol^{-1}, of the substrate– adsorbate configuration. The total energy is defined as the sum of the energies of the adsorbate components, the rigid adsorption energy and the deformation energy. In this study, the substrate energy

(iron surface) is taken as zero. In addition, adsorption energy in kJ mol^{-1} reports energy released (or required) when the relaxed adsorbate components (furan derivatives) are adsorbed on the substrate. The adsorption energy is defined as the sum of the rigid adsorption energy and the deformation energy for the adsorbate components. The rigid adsorption energy reports the energy, in kJ mol^{-1}, released (or required) when the unrelaxed adsorbate components (i.e., before the geometry optimization step) are adsorbed on the substrate. The deformation energy reports the energy, in kJ mol^{-1}, released when the adsorbed adsorbate components are relaxed on the substrate surface. Table 8 shows also (dE$_{ads/dNi}$), which reports the energy, in kJ mol^{-1}, of substrate– adsorbate configurations where one of the adsorbate components has been removed. High values of adsorption energy indicate that the molecule will give the highest inhibition efficiency. The shape of the molecule on metal surface shown in Fig.16.

Table 8 . The calculated descriptors obtained from molecular dynamics calculations.

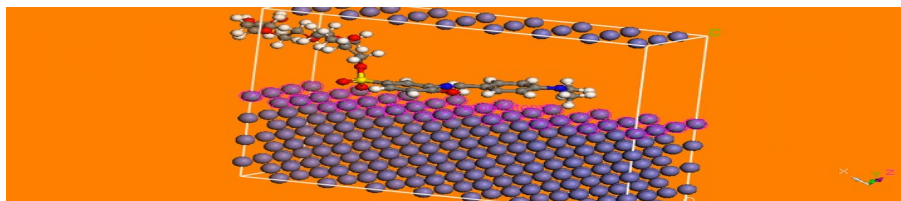| Total energy kJ mol^{-1}	Adsorption energy kJ mol^{-1}	Rigid adsorption energy kJ mol^{-1}	Deformation energy kJ mol^{-1}	dEads/dNi kJ mol^{-1}
-325.68	-777.12	-329.798	-447.32	-777.12
-323.94	-775.37	-335.38	-439.98	-775.37
-321.55	-772.98	-331.48	-441.49	-772.98
-321.07	-772.50	-336.56	-435.94	-772.50

Fig.16. Molecular simulations for the most favorable modes of adsorption obtained for the investigated inhibitors on Fe (1 1 1) surface.

References:

1. G. Schmitt, Application of inhibitors for acid media, J.Brit. Corros. , **19** (1984) 165.

2. F. Bentiss, M. Lagrenee, M. Traisnel and J.C. Hornez, Corros. Sci., **41** (1999) 789–803.

3. F.B. Growcock,W.W. Frenier and P.A. Andreozzi, Corrosion , **45** (1989) 1007–1015.

4. I. Lukovits, E. Kalman and G. Palinkas, Corrosion, **51** (1995) 201–205.

5. R.C. Ayers Jr., N. Hackerman and J. Electrochem. Soc., **110** (1963) 507–513.

6. G. Gece, Corros. Sci., **50** (2008) 2981.

7. H.J. Henriquez-Roman, L. Padilla-Campos, M.A. Paez, J.H. Zagal, M.A. Rubio, C.M. Rangel, J. Costamagna and G. Cardenas-Jiron, J. Mol. Struct. (THEOCHEM), **757** (2005) 1.

8. N. Khalil, Electrochim. Acta, **48** (2003) 2635.

9. M. Behpour, S.M. Ghoreishi, N. Soltani, M. Salavati-Niasari, M. Hamadanian and A. Gandomi, Corros. Sci., **50** (2008) 2172.

10. M.K. Awad, R.M. Issa and F.M. Atlam, Mater. Corros., **60** (2009) 813.

11. M.K. Awad, J. Electroanal. Chem., **567** (2004) 219.

12. I.N. Levine, Quantum Chemistry, Prentice Hall, New Jersey, (1991).

13. M.A. Hegazy, Corros. Sci., **51** (2009) 2610–2618.

14. Gaussian 09, Revision A.02, M. J. Frisch, G. W. Trucks, H. B. Schlegel, G. E. Scuseria, M. A. Robb, J. R. Cheeseman, G. Scalmani, V. Barone, B. Mennucci, G. A. Petersson, H. Nakatsuji, M. Caricato, X. Li, H. P. Hratchian, A. F. Izmaylov, J. Bloino, G. Zheng, J. L. Sonnenberg, M. Hada, M. Ehara, K. Toyota, R. Fukuda, J. Hasegawa, M. Ishida, T. Nakajima, Y. Honda, O. Kitao, H. Nakai, T. Vreven, J. A. Montgomery, Jr., J. E. Peralta, F. Ogliaro, M. Bearpark, J. J. Heyd, E. Brothers, K. N. Kudin, V. N. Staroverov, R. Kobayashi, J. Normand, K. Raghavachari, A. Rendell, J. C. Burant, S. S. Iyengar, J. Tomasi, M. Cossi, N. Rega, J. M. Millam, M. Klene, J. E. Knox, J. B. Cross, V. Bakken, C. Adamo, J. Jaramillo, R. Gomperts, R. E. Stratmann, O. Yazyev, A. J. Austin, R. Cammi, C. Pomelli, J. W. Ochterski, R. L. Martin, K. Morokuma, V. G. Zakrzewski, G. A. Voth, P. Salvador, J. J. Dannenberg, S. Dapprich, A. D. Daniels, O. Farkas, J. B. Foresman, J. V. Ortiz, J. Cioslowski, and D. J. Fox, Gaussian, Inc., Wallingford CT, (2009).

15. V.S. Sastri and J.R. Perumareddi, Corrosion, **53** (1996) 671.

16. R.G. Pearson, Inorg. Chem., **27** (1988) 734.

17. J. Barriga, B. Coto and B. Fernandez, Tribol. Int., **40** (2007) 960.

18. H. Sun, P. Ren and J.R. Fried, Comput. Theor. Polym. Sci., **8** (1998) 229.

19. U.R. Evans, The Corrosion of Metals, Edward Arnold, London, (1960). p. 898.

20. J.O.M. Bockris and L.J.V. Minevski, Protection of aluminium by means of transition metal alloys, J. Electroanal. Chem., **349** (1993) 375–414.

21. O.L. Riggs Jr., Corrosion Inhibitors, 2nd ed., C.C. Nathan, Houston, TX, (1973).

22. A. A. El-Sayed, Corros. Prev. Control, **43** (1996) 23–27.

23. L.B. Tang, G.N. Mu and G.H. Liu, Corros. Sci., **45** (2003) 2251.

24. P. Manjula, S. Manonmani, P. Jayaram and S. Rajendran, Anti-Corros. Methods Mater., **48** (2001) 319.

25. S.S. Abdel-Rehim, A.M. Magdy and K.F. Khaled, Mater. Chem. Phys., **70** (2001) 268.

26. G. Quartarone, M. Battilana, L. Bonaldo and T. Tortato, Corros. Sci. **50** (2008) 3467–3474.

27. M.A. Hegazy, H.M. Ahmed and A.S. El-Tabei, Corros. Sci., **53** (2011) 671–678.

28. L. Finar, Organic chemistry, 6th Ed., Vol. 1, Longman, (1986).

29. G.N. Mu, X.H. Li, Q. Qu and J. Zhou, Acta Chim. Sinica, **62** (2004) 2386–2394.

30. J.M. Thomas, W.J. Thomas, Introduction to the Principles of Heterogeneous Catalysis, fifth ed., Academic Press, London, (1981), p. 14.

31. J. Fang, J. Li and J. Mol. Struct. (THEOCHEM), **593** (2002) 179–185.

32. S. Ramachandran, B.L. Tsai, M. Blanco, H. Chen, Y. Tang and W.A. Goddard III, J. Phys. Chem. A, **101** (1997) 83–91.